

Supporting Information for

Dioxygen-Initiated Oxidation of Heteroatomic
Substrates Incorporated into Ancillary Pyridine
Ligands of Carboxylate-Rich Diiron(II) Complexes

*Emily C. Carson and Stephen J. Lippard**

Department of Chemistry, Massachusetts Institute of Technology, Cambridge, Massachusetts
02139

lippard@mit.edu

RECEIVED DATE August 00, 2005

Table S1. Summary of X-ray Crystallographic Data.

	3·C₂H₄Cl₂	4·1.5C₂H₄Cl₂/C₅H₁₂	5·C₆H₅Cl
Empirical Formula	Fe ₂ C ₉₅ H ₆₂ NO ₈ F ₈ PCl ₂	Fe ₂ C ₉₈ H ₉₃ NO ₈ SCl ₃	Fe ₂ C ₁₀₈ H ₉₂ N ₂ O ₁₀ S ₂ Cl ₂
Formula Weight	1711.03	1662.84	1824.56
Space Group	P $\bar{1}$	P2 ₁ /c	P $\bar{1}$
a, Å	13.6676(14)	13.0032(6)	12.3481(13)
b, Å	14.0155(14)	26.3878(12)	13.2842(13)
c, Å	21.278(2)	24.6935(12)	14.8486(16)
α , deg	80.799(2)		107.009(2)
β , deg	89.079(2)	95.8440(10)	103.260(2)
γ , deg	86.533(2)		95.274(3)
V, Å ³	4016.0(7)	8428.9(7)	2233.7(4)
Z	2	4	1
ρ_{calc} , g/cm ³	1.415	1.310	1.356
T, °C	-100	-100	-100
μ (Mo K α), mm ⁻¹	0.526	0.523	0.495
θ limits, deg	1.47 – 26.73	1.66 – 27.10	1.63 – 26.02
total no. of data	33796	72962	18030
no. of unique data	16744	18576	8699
no. of params	1099	1279	572
Goodness-of-fit on F ²	1.030	1.196	0.769
R1 ^a	0.0709	0.0786	0.0744
wR ^{2b}	0.1767	0.1679	0.0999
max, min peaks, e/Å ³	1.124, -1.036	1.031, -0.610	0.463, -0.323

$$^a R1 = \frac{\sum ||F_o| - F_c||}{\sum |F_o|} \quad ^b wR^2 = \left\{ \frac{\sum [w(F_o^2 - F_c^2)^2]}{\sum [w(F_o^2)^2]} \right\}^{1/2}$$

Table S1. Continued.

	6	7·4CH₂Cl₂	8·3CH₂Cl₂
Empirical Formula	FeC ₅₂ H ₄₄ N ₂ O ₄ S ₂	Fe ₆ C ₁₂₂ H ₁₁₀ N ₂ O ₁₈ P ₂ Cl ₁₂	Fe ₂ C ₉₆ H ₆₈ NO ₁₂ F ₈ PCl ₆
Formula Weight	880.86	2714.56	1934.88
Space Group	P2 ₁ /c	P $\bar{1}$	P $\bar{1}$
a, Å	18.821(19)	14.508(2)	12.9063(17)
b, Å	12.262(12)	15.852(2)	14.1811(18)
c, Å	21.18(2)	15.904(3)	24.990(3)
α , deg		78.407(3)	78.235(3)
β , deg	115.123(16)	77.951(3)	86.110(2)
γ , deg		63.832(3)	86.837(3)
V, Å ³	4425(8)	4042(9)	4463.4(10)
Z	4	1	2
ρ_{calc} , g/cm ³	1.322	1.415	1.440
T, °C	-100	-100	-100
μ (Mo K α), mm ⁻¹	0.483	1.004	0.602
θ limits, deg	1.95 – 27.16	1.64 – 25.00	1.67 – 27.10
total no. of data	37528	23654	39033
no. of unique data	9779	11127	19334
no. of params	550	730	1151
Goodness-of-fit on F ²	1.131	0.997	0.997
R1 ^a	0.0566	0.1032	0.0855
wR ^{2b}	0.1240	0.1826	0.1521
max, min peaks, e/Å ³	0.505, -0.278	1.028, -0.551	0.779, -0.721

$$^a R1 = \frac{\sum ||F_o| - F_c||}{\sum |F_o|} \quad ^b wR^2 = \left\{ \frac{\sum [w(F_o^2 - F_c^2)^2]}{\sum [w(F_o^2)^2]} \right\}^{1/2}$$

Table S2. Selected Interbond Lengths and Angles for $[\text{Fe}_2(\mu\text{-O}_2\text{CAr}^{\text{Tol}})_2(\text{O}_2\text{CAr}^{\text{Tol}})_2\text{-}(2\text{-MeS(O)py})_2]$ (**5**)^a

	Bond Length (Å)		Bond Angle (deg)	
Fe1...Fe2	4.586(2)	O1-Fe1-N1	79.1(3)	
Fe1-N1	2.156(6)	O2-Fe1-N1	96.7(2)	
Fe1-O1	2.234(5)	O3-Fe1-N1	92.4(2)	
Fe1-O2	1.961(5)	O4-Fe1-N1	83.62(18)	
Fe1-O3	2.071(5)	O5-Fe1-N1	149.98(19)	
Fe1-O4	2.160(5)	O1-Fe1-O2	82.09(19)	
Fe1-O5	2.267(5)	O1-Fe1-O3	171.5(2)	
		O1-Fe1-O4	83.7(2)	
		O1-Fe1-O5	97.75(17)	
		O2-Fe1-O3	98.6(2)	
		O2-Fe1-O4	163.3(2)	
		O2-Fe1-O5	112.7(2)	
		O3-Fe1-O4	96.08(18)	
		O3-Fe1-O5	89.31(17)	
		O4-Fe1-O5	59.28(17)	

^aNumbers in parentheses are estimated standard deviations of the last significant figure. Atoms are labeled as indicated Figures 1 and S4.

Table S3. Selected Interbond Distances and Angles for $[\text{Fe}_2(\text{O}_2\text{CAr}^{\text{Tot}})_2(2\text{-HSpY})_2]$ (**6**)^a

	Bond Length (Å)		Bond Angle (deg)
Fe1–O1	2.052(2)	O1–Fe1–S1	102.69(8)
Fe1–O3	2.029(3)	O1–Fe1–S2	110.22(6)
Fe1–S1	2.398(2)	O3–Fe1–S1	112.35(5)
Fe1–S2	2.398(3)	O3–Fe1–S2	98.59(6)
N1–C1	1.348(3)	O1–Fe1–O3	133.35(9)
C1–C2	1.407(4)	S1–Fe1–S2	92.04(2)
C2–C3	1.367(4)	Fe1–S1–C6	108.93(9)
C3–C4	1.393(4)	Fe1–S2–C6	106.95(9)
C4–C5	1.355(4)		
C5–N1	1.353(4)		
S1–C1	1.716(3)		
N2–C6	1.346(3)		
C6–C7	1.412(4)		
C7–C8	1.363(4)		
C8–C9	1.394(4)		
C9–C10	1.364(4)		
C10–N2	1.346(3)		
S2–C6	1.717(3)		
N1···O4	2.747(3)		
N2···O2	2.706(3)		

^aNumbers in parentheses are estimated standard deviations of the last significant figure. Atoms are labeled as indicated Figures 1 and S6.

Table S4. Summary of the Conditions and Amount of Oxidation Product Isolated for the Reaction of Compounds **2**, **4**, and **5** with Dioxygen in CH₂Cl₂.

Compound	[Fe ₂] (mM)	Reaction Time (h)	% Oxidized Ligand Recovered ^a
2	8.6	1.5	29
4	8.2	1.5	58
5	5.1	16	40

^aBased on [Fe₂]

Table S5. Summary of conditions and amount of oxidation product isolated for the reaction of **1** and **3** with additional equiv of phosphine and dioxygen

[Fe ₂] (mM)	Compound	Equiv 2-Ph ₂ Ppy Added	Reaction Time (h)	Equiv 2-Ph ₂ P(O)py Recovered ^a
2.5	1	8.44	1	3.98
1.4	1	47.0	13	13.4
0.31	1	51.5	17	17.0
3.2	3	8.55	17	2.95
		Equiv PPh ₃ Added		Equiv (O)PPh ₃ Recovered
0.42	1	5.62	14	0.70

^aIncluding 1 equiv of 2-Ph₂Ppy from [Fe₂].

Table S6. Selected Interatomic Distances (Å) and Angles (deg) for [Fe₆(μ₄-O)₂(μ-OH)₆-(μ-O₂CAr^{Tol})₄Cl₄(2-Ph₂P(O)py)₂] (7)^a

Fe1–O1	2.010(7)	Fe2–O3	1.993(6)	Fe3–O2	1.890(7)
Fe1–O2	2.036(6)	Fe2–O3A	1.990(6)	Fe3–O3	2.260(6)
Fe1–O3	1.911(6)	Fe2–O6	2.036(6)	Fe3–O7A	1.922(6)
Fe1–O4	2.049(6)	Fe2–O7	2.022(6)	Fe3–O9	1.898(6)
Fe1–O5	2.044(6)	Fe2–O8	2.007(6)	Fe3–Cl2	2.215(3)
Fe1–Cl1	2.290(3)	Fe2–O9	2.007(6)	Fe3···Fe2	3.143(2)
Fe1–Fe3	3.157(2)	Fe2···Fe2A	3.029(3)	Fe3A···Fe2	3.158(2)
O1–Fe1–Cl1	95.8(2)	O3–Fe2–O3A	81.0(3)	Cl2–Fe3–O2	104.9(2)
O2–Fe1–Cl1	176.8(2)	O3–Fe2–O6	98.5(3)	Cl2–Fe3–O3	177.57(19)
O3–Fe1–Cl1	97.0(2)	O3–Fe2–O7	101.6(3)	Cl2–Fe3–O7A	101.9(2)
O4–Fe1–Cl1	91.7(2)	O3–Fe2–O8	164.8(3)	Cl2–Fe3–O9	105.9(2)
O5–Fe1–Cl1	89.4(2)	O3–Fe2–O9	80.5(3)	O2–Fe3–O3	74.9(2)
O1–Fe1–O2	87.1(3)	O6–Fe2–O3A	164.3(3)	O2–Fe3–O7A	117.2(3)
O1–Fe1–O3	167.1(3)	O6–Fe2–O7	84.2(3)	O2–Fe3–O9	115.5(3)
O1–Fe1–O4	84.9(3)	O6–Fe2–O8	87.6(3)	O3–Fe3–O7A	76.2(2)
O1–Fe1–O5	84.3(3)	O6–Fe2–O9	93.9(3)	O3–Fe3–O9	76.3(2)
O2–Fe1–O3	80.0(3)	O7–Fe2–O3A	80.6(3)	O9–Fe3–O7A	109.7(3)
O2–Fe1–O4	89.8(3)	O7–Fe2–O8	92.7(3)		
O2–Fe1–O5	89.7(3)	O7–Fe2–O9	177.3(3)		
O3–Fe1–O4	95.2(3)	O8–Fe2–O3A	96.89(3)		
O3–Fe1–O5	95.2(3)	O8–Fe2–O9	85.3(3)		
O4–Fe1–O5	169.3(3)	O9–Fe2–O3A	101.5(3)		

^aNumbers in parentheses are estimated standard deviations of the last significant figure. Atoms are labeled as indicated Figures 4 and S9.

Table S7. Bond Valence Sum Analysis of Iron-Ligand Bonds in **7** and **8**

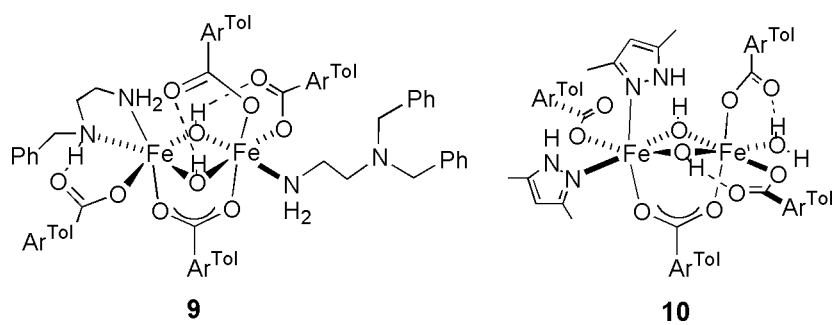
Bond	Bond Length (Å)	Bond Valence	Bond Valence Sum
[Fe₆(μ₄-O)₂(μ-OH)₆(μ-O₂CAr^{1ol})₄Cl₄(2-Ph₂P(O)py)₂] (7)			
Fe1-O1	2.010(7)	0.507	3.306
Fe1-O2	2.036(6)	0.473	
Fe1-O3	1.911(6)	0.663	
Fe1-O4	2.049(6)	0.457	
Fe1-O5	2.044(6)	0.463	
Fe1-Cl1	2.290(3)	0.743	

Fe2-O3	1.993(6)	0.531	3.054
Fe2-O3A	1.990(6)	0.536	
Fe2-O6	2.036(6)	0.473	
Fe2-O7	2.022(6)	0.491	
Fe2-O8	2.007(6)	0.512	
Fe2-O9	2.007(6)	0.512	

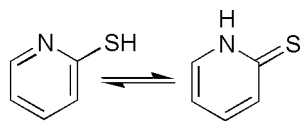
Fe3-O2	1.890(7)	0.702	3.20
Fe3-O3	2.260(6)	0.258	
Fe3-O7A	1.922(6)	0.644	
Fe3-O9	1.898(6)	0.687	
Fe3-Cl2	2.215(3)	0.910	
[Fe₂(μ-OH)₂(μ-O₂CAr^{4-FPh})(O₂CAr^{4-FPh})₃(OH₂)(2-Ph₂P(O)py)] (8)			
Fe1-N1	2.210(4)	0.383	3.131
Fe1-O1	2.023(3)	0.490	
Fe1-O2	1.954(4)	0.590	
Fe1-O3	1.981(4)	0.549	
Fe1-O5	2.003(3)	0.517	
Fe1-O7	1.947(3)	0.602	

Fe2-O2	1.981(4)	0.549	3.118
Fe2-O3	1.977(4)	0.555	
Fe2-O4	2.097(4)	0.401	
Fe2-O6	2.017(3)	0.498	
Fe2-O9	1.974(3)	0.559	
Fe2-O11	1.976(3)	0.556	

Chart S1



Scheme S1



Captions for Supporting Figures

Figure S1. Top: ORTEP diagram of $[\text{Fe}_2(\mu\text{-O}_2\text{CAr}^{4\text{-FPh}})_3(\text{O}_2\text{CAr}^{4\text{-FPh}})(2\text{-Ph}_2\text{Ppy})]$ (**3**) illustrating 50% probability thermal ellipsoids for all non-hydrogen atoms. Bottom: Drawing in which the aromatic rings of the $\text{O}_2\text{CAr}^{4\text{-FPh}}$ ligands are omitted for clarity.

Figure S2. FT-IR spectra of KBr pellets of $[\text{Fe}_2(\mu\text{-O}_2\text{CAr}^{4\text{-FPh}})_3(\text{O}_2\text{CAr}^{4\text{-FPh}})(2\text{-Ph}_2\text{Ppy})]$ (**3**) (top) and $[\text{Fe}_2(\mu\text{-OH})_2(\mu\text{-O}_2\text{CAr}^{4\text{-FPh}})(\text{O}_2\text{CAr}^{4\text{-FPh}})_3(\text{OH}_2)(2\text{-Ph}_2\text{P(O)py})]$ (**8**) (bottom).

Figure S3. Top: ORTEP diagram of $[\text{Fe}_2(\mu\text{-O}_2\text{CAr}^{\text{Tol}})_3(\text{O}_2\text{CAr}^{\text{Tol}})(2\text{-MeSpy})]$ (**4**) showing 50% probability thermal ellipsoids for all non-hydrogen atoms. Bottom: Drawing in which the aromatic rings of $\text{O}_2\text{CAr}^{\text{Tol}}$ are omitted for clarity.

Figure S4. Top: ORTEP diagram of $[\text{Fe}_2(\mu\text{-O}_2\text{CAr}^{\text{Tol}})(\text{O}_2\text{CAr}^{\text{Tol}})_2(2\text{-MeS(O)py})_2]$ (**5**) showing 50 % probability thermal ellipsoids for all non-hydrogen atoms. Bottom: Drawing in which the aromatic rings of $\text{O}_2\text{CAr}^{\text{Tol}}$ are omitted for clarity.

Figure S5. FT-IR spectra of KBr pellets of $[\text{Fe}_2(\mu\text{-O}_2\text{CAr}^{\text{Tol}})_3(\text{O}_2\text{CAr}^{\text{Tol}})(2\text{-MeSpy})]$ (**4**) (top) and $[\text{Fe}_2(\mu\text{-O}_2\text{CAr}^{\text{Tol}})_2(\text{O}_2\text{CAr}^{\text{Tol}})_2(2\text{-MeS(O)py})_2]$ (**5**) (bottom). The arrow designates $\nu_{\text{S-O}}$.

Figure S6. Top: ORTEP diagram of $[\text{Fe}(\text{O}_2\text{CAr}^{\text{Tol}})_2(2\text{-HSpy})_2]$ (**6**) showing 50 % probability thermal ellipsoids for all non-hydrogen atoms. Bottom: Drawing in which the aromatic rings of $\text{O}_2\text{CAr}^{\text{Tol}}$ are omitted for clarity.

Figure S7. FT-IR spectrum of a KBr pellet of $[\text{Fe}(\text{O}_2\text{CAr}^{\text{Tol}})_2(2\text{-HSpy})_2]$ (**6**).

Figure S8. Mössbauer spectrum (experimental data (|), calculated fit (—)) recorded at 4.2 K for a solid sample of $[\text{Fe}_2(\mu\text{-O}_2\text{CAr}^{4\text{-FPh}})_3(\text{O}_2\text{CAr}^{4\text{-FPh}})(2\text{-Ph}_2\text{Ppy})]$ (**3**).

Figure S9. Top: ORTEP diagram of $[\text{Fe}_6(\mu_4\text{-O})_2(\mu\text{-OH})_6(\mu\text{-O}_2\text{CAr}^{\text{Tol}})_4\text{Cl}_4(2\text{-Ph}_2\text{P(O)py})_2]$ (**7**) illustrating 50% probability thermal ellipsoids for all non-hydrogen atoms. Bottom: Drawing in which the aromatic rings of the $\text{O}_2\text{CAr}^{\text{Tol}}$ ligands are omitted for clarity.

Figure S10. Top: ORTEP diagram of $[\text{Fe}_2(\mu\text{-OH})_2(\mu\text{-O}_2\text{CAr}^{4\text{-FPh}})(\text{O}_2\text{CAr}^{4\text{-FPh}})_3(\text{OH}_2)(2\text{-Ph}_2\text{P(O)py})]$ (**8**) illustrating 50% probability thermal ellipsoids for all non-hydrogen atoms. Bottom: Drawing in which the aromatic rings of the $\text{O}_2\text{CAr}^{4\text{-FPh}}$ ligands are omitted for clarity.

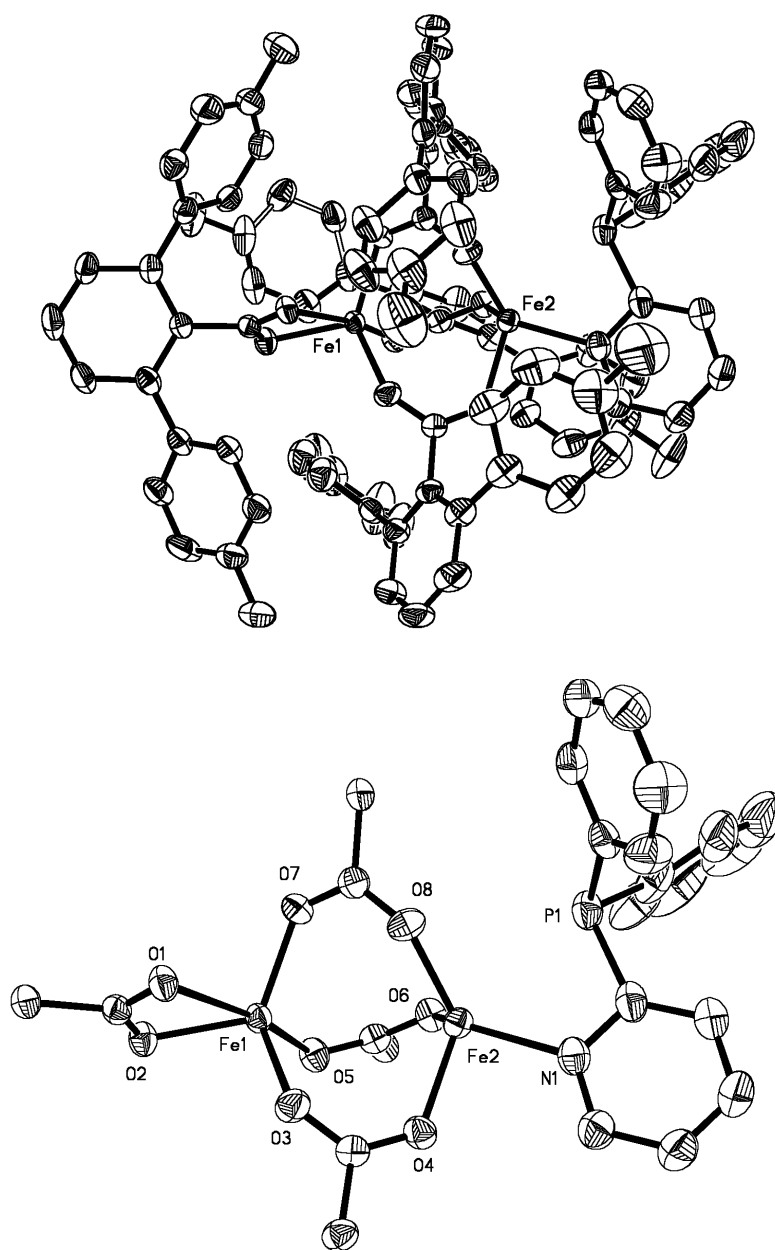


Figure S1. Carson and Lippard

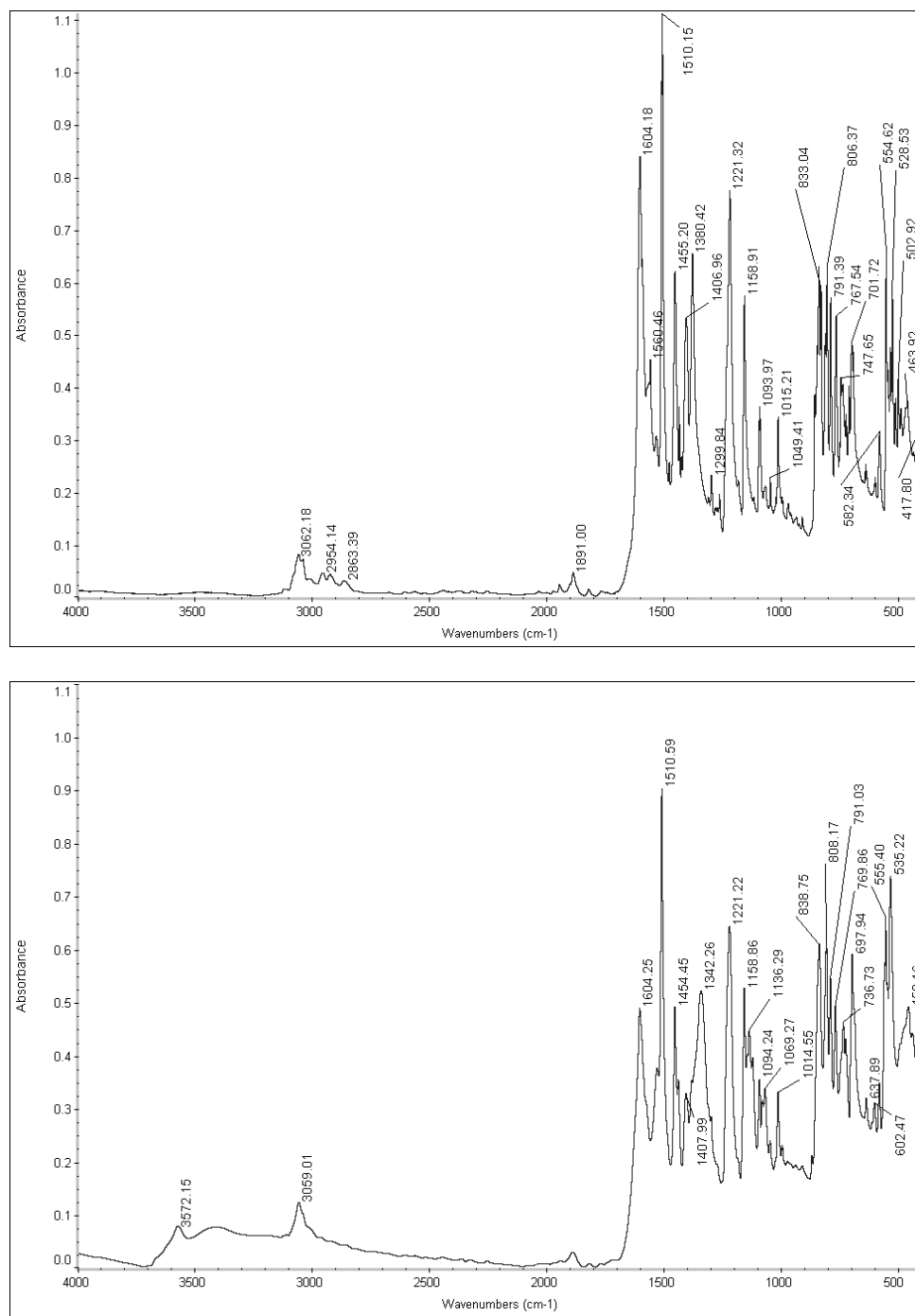


Figure S2. Carson and Lippard

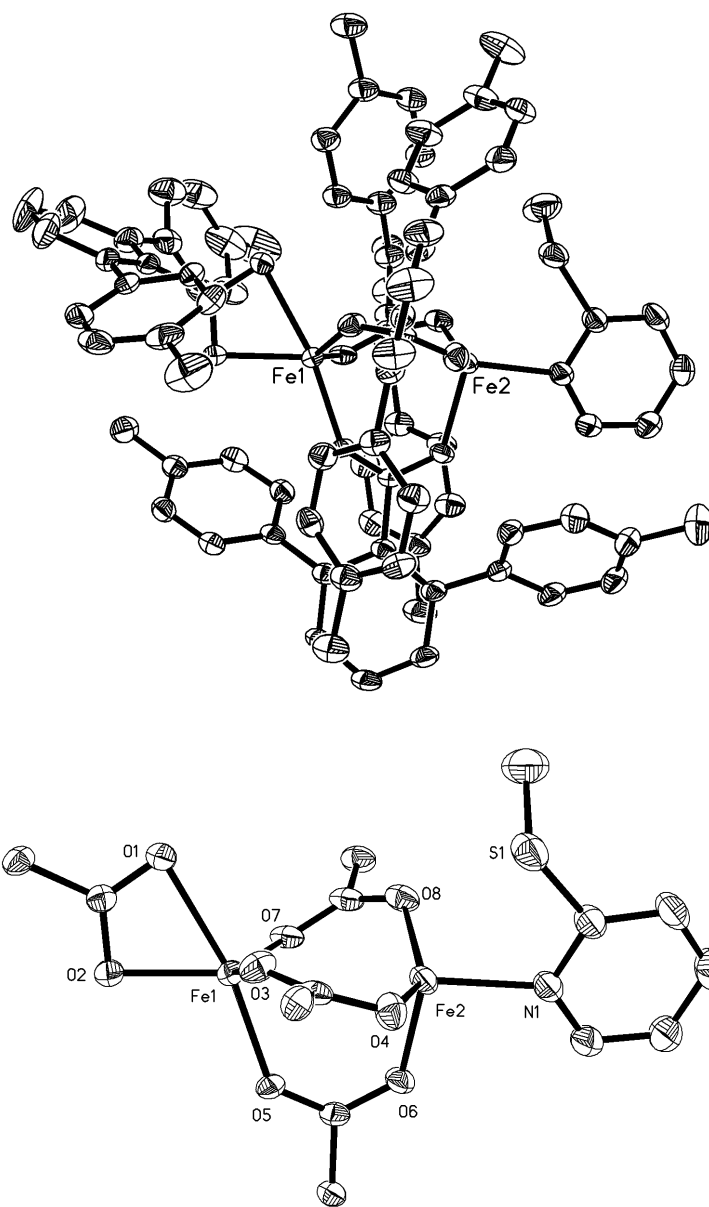


Figure S3. Carson and Lippard

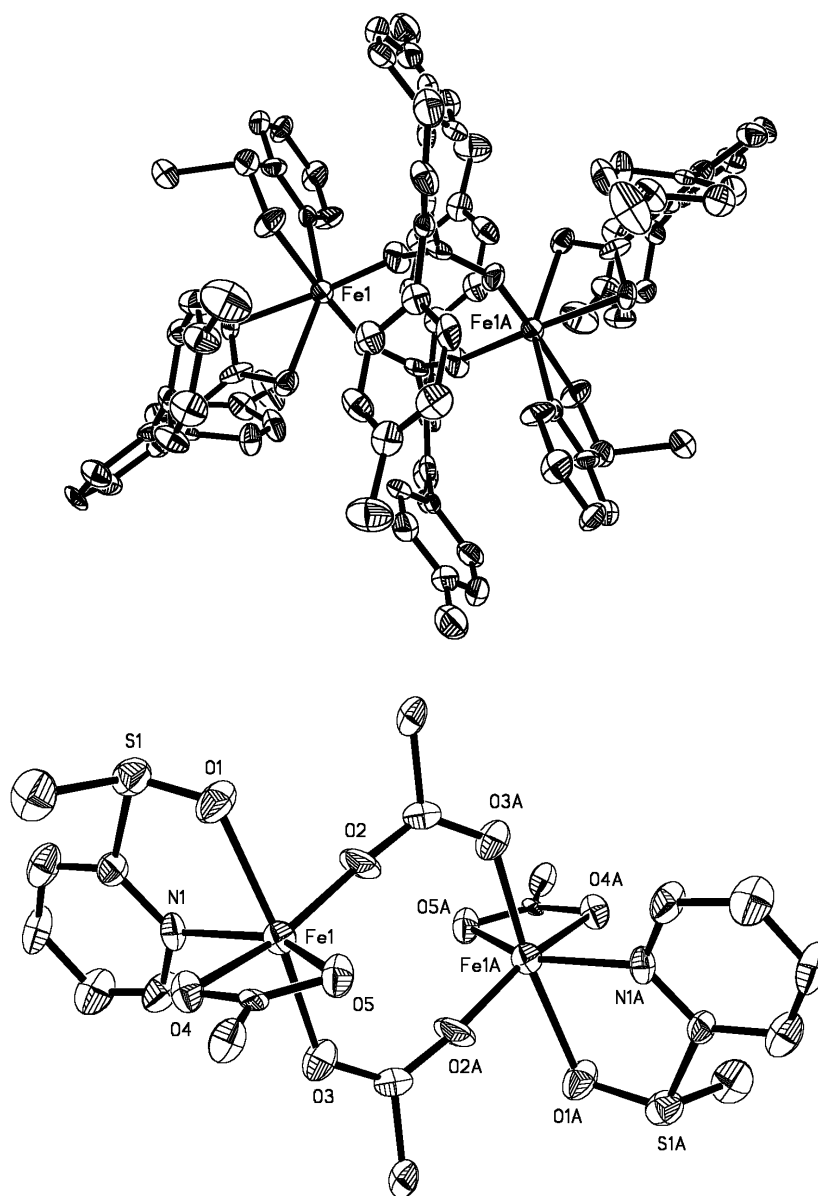


Figure S4. Carson and Lippard

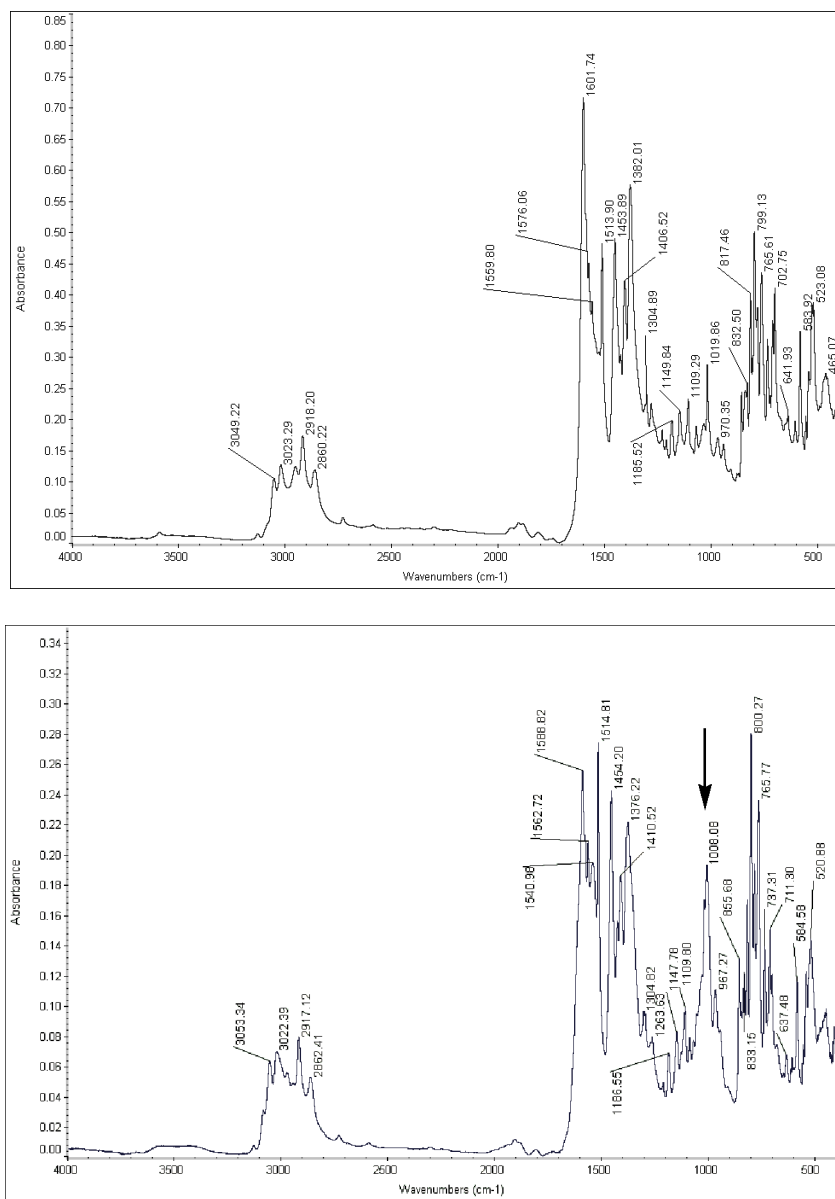


Figure S5. Carson and Lippard

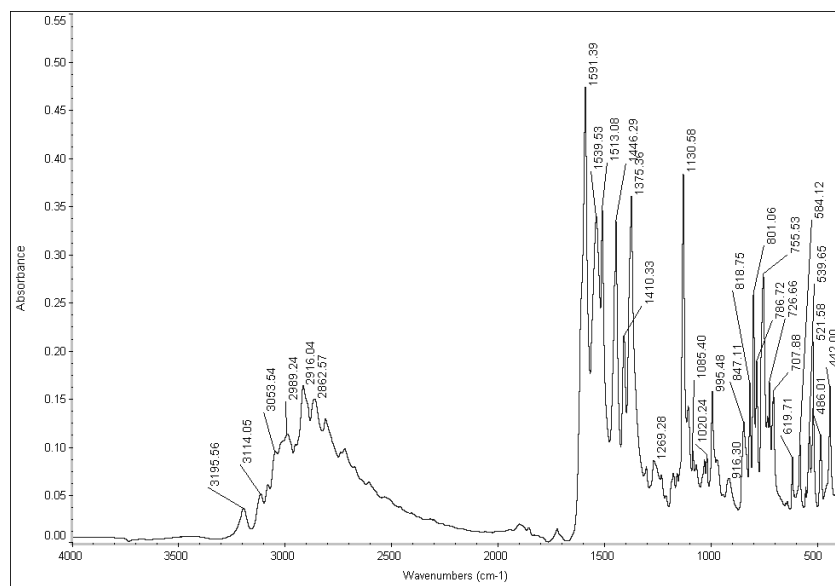


Figure S7. Carson and Lippard

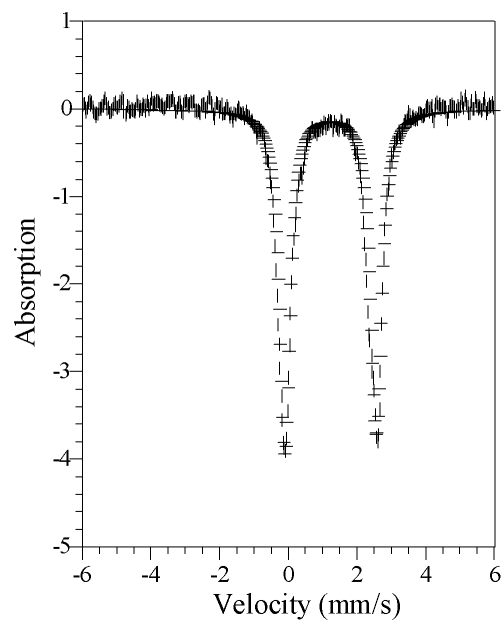


Figure S8. Carson and Lippard

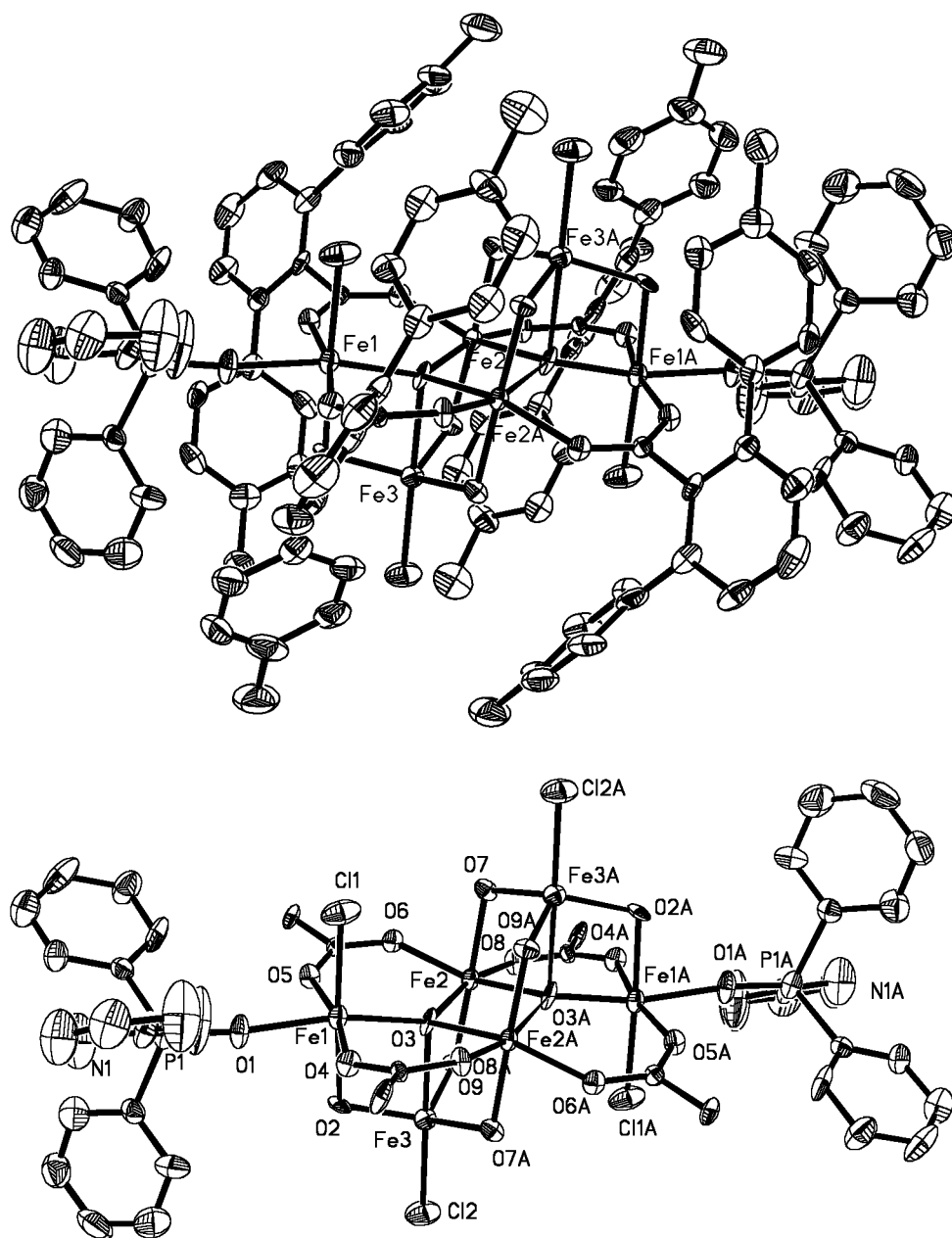


Figure S9. Carson and Lippard

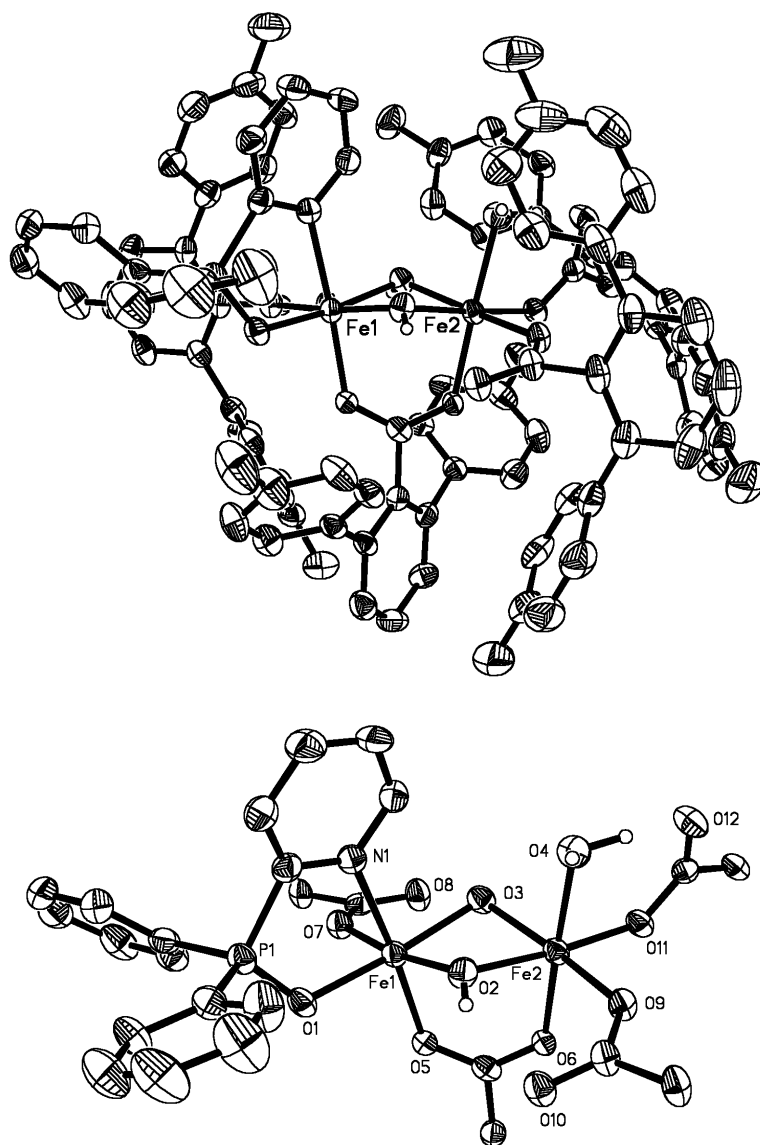


Figure S10. Carson and Lippard